

## MULTISCALE BALANCE OF EXCITATION AND INHIBITION IN SINGLE-UNIT ENSEMBLE RECORDINGS IN HUMAN AND MONKEY NEOCORTEX

NIMA DEGHANI<sup>1,2</sup> ADRIEN PEYRACHE<sup>3</sup> BARTOSZ TELENCZUK<sup>2</sup> MICHEL LE VAN QUYEN<sup>4</sup> ERIC HALGREN<sup>5</sup>  
SYD S. CASH<sup>6</sup> NICHOLAS G. HATSOPOULOS<sup>7</sup> ALAIN DESTEXHE<sup>2</sup>

1. Wyss Institute for Biologically-Inspired Engineering, Harvard University, USA.
2. Laboratory of Computational Neuroscience, Unit de Neurosciences, Information et Complexit, CNRS, France.
3. NYU Neuroscience Institute and Center for Neural Sciences, New York University, USA.
4. Centre de Recherche de l'Institut du Cerveau et de la Moelle pinire (CRICM), UPMC, France.
5. Multimodal Imaging Laboratory, Departments of Neurosciences and Radiology, University of California San Diego, USA.
6. Department of Neurology, Massachusetts General Hospital and Harvard Medical School, USA.
7. Department of Organismal Biology and Anatomy, Committee on Computational Neuroscience, University of Chicago, USA.

*Draft version December 7, 2024*

### ABSTRACT

High-density ensemble recordings from the neocortex of human and monkey were used to categorize large ensembles of units into regular-spiking (RS) and fast-spiking (FS) cells based on spike waveform features and functional interactions. We adapted renormalization methods to evaluate the static and dynamic aspects of multiscale balance of these two interacting groups of cells. We found that the distribution of ensemble magnitude is similar for FS and RS cells at all scales, demonstrating that excitatory and inhibitory activity are well balanced. Scaling the ensemble series to a matrix of E-I ensemble pairs, enabled us to quantify the fine details of dynamic features of excitation and inhibition in each brain state and in comparison to one another. Minor deviations were found for light slow-wave sleep (SWS), Rapid Eye Movement (REM) sleep, and wakefulness, with moderate deviations from the plane of symmetry and absolute balance found for deep SWS. In contrast, we observed a complete break-down of this balanced activity during instances of focal seizures. In conclusion, large ensemble of units show a remarkable excitatory and inhibitory balance, at multiple temporal scales, and for all brain states, except seizures, showing that balanced excitation-inhibition is a fundamental feature of normal brain activity.

### 1. INTRODUCTION

Balanced excitation/inhibition (E/I) is not only considered to be a functional cornerstone in the cerebral cortex, but also has been hypothesized to play a major role in areas other than cortex (Okun *et al.* 2010). The role of balance in neocortical processing was first suggested theoretically (Shadlen & Newsome 1994; Vreeswijk & Sompolinsky 1996). Later experimental evidence, in vitro (Shu *et al.* 2003) and in vivo (Haider *et al.* 2006) became the basis for the claim that a fundamental property of cortical processing lies in balanced inhibition and excitation. The concept of balanced networks was further extended to its influence on maximizing information capacity and information transmission in terms of neural avalanches (Shew *et al.* 2011; Lombardi *et al.* 2012). Such multiscale aspects of neural computations is reminiscent of state transitions in other physical systems, which also involve many different scales Wilson (1979). Whether or not the two inhibitory and excitatory systems interact in a balanced way over many different scales of computation, is presently unknown. In this paper, we address this question by taking advantage of recent advances in the recording and separation between excitatory and inhibitory cells (Barthó *et al.* 2004; Peyrache *et al.* 2012) to characterize the dynamics of excitatory and inhibitory populations, in human recordings (temporal cortex), and monkey recordings (motor and premotor cortex). The units were initially clustered based on spike shape, and in a next step,

their excitatory or inhibitory character could be confirmed by their functional interactions, as determined using cross-correlograms (Peyrache *et al.* 2012). This procedure provides, for the first time in humans, a coherent separation between excitatory (fast-spiking, FS) and inhibitory (regular-spiking, RS) cells, where their excitatory or inhibitory nature could be proven. This was only possible because of the long period of the recordings (several segments of continuous 12-hour recordings for each subject). A similar discrimination between RS and FS cells was also done for the monkey recordings using a similar electrode array (Bartosiz Telenczuk, in preparation). Together, these human and monkey recordings provide a unique data set where one can investigate the dynamics of excitation and inhibition in different brain states. In the present paper, we characterize this dynamics by renormalizing the temporal structure of ensemble inhibition and excitation, analyzing their interaction in different brain states and showing situations when the balance breaks down.

### 2. RESULTS

#### 2.1. Sample Recordings and categorization of cell population

We first show the dynamic balance between excitatory and inhibitory cell activities in all different brain states, in human and monkey. We then use a number of methods to quantify this balance at different temporal scales, as well as the deviations from balanced activity. Finally, we show an example of a pathological brain state where the balance breaks down.

Figure 1 shows raw traces of local field potential (LFP) during slow-wave sleep (SWS) from both monkey and human. Along with the LFP, the rasters show the activity of single units divided into RS (blue) and FS (red) cells. We use this categorized ensemble activity to quantify the neocortical balance of excitation and inhibition.

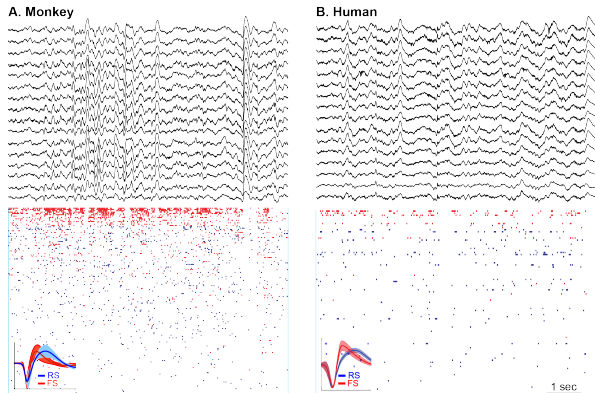


FIG. 1.— Sample recordings from a UTAH multielectrode array in Monkey (A) PMD and Human (B) Temporal cortices during 8 sec of SWS (Slow-wave sleep). In each panel, the upper section depicts LFP (local field potentials) from different locations of the multielectrode array. Lower sections show the corresponding Excitatory (blue) and Inhibitory (red) cells. Insets show the spike-waveform that was used to categorize the units into two inhibitory and excitatory cell populations.

## 2.2. Recordings from different states are suggestive of excitatory and inhibitory balance

A consistent observation for different states is that the inhibition and excitation mirror each other (Fig.2 and supplementary Fig.8, note the normalized histograms of ensemble activity). One can see from the overall firing patterns (bottom), that in general an increase or decrease of the excitatory population is mirrored by a similar dynamics among inhibitory cells, sometimes with a slight delay (see below for quantification).

This observation leads to question whether such possible balance extends throughout all times. Moreover, is it the case that the fluctuations of excitation and inhibition mirror each other throughout at a multitude of time scales, or not? And, what happens when the system loses its capability to preserve balance between excitation and inhibition. In what follows, we aim to decipher such possible relation between excitation and inhibition and we provide a quantitative signature of probable multiscale balance.

## 2.3. Dynamic and Static aspects of balance

### 2.3.1. Preservation of balance across scales

To test balance across multiple temporal scales, we defined 32 different scales ranging from a few milliseconds to many decades of seconds (as shown in Fig.3.A). A multi-step zoom across some scales shows that ensemble excitation and inhibition keep each other in a checked state at many lengths of computation. An example shown in Fig.3, panels C1 through C5, shows that when the firing of a given category is normalized to the total related ensemble firing power, excitation and inhi-

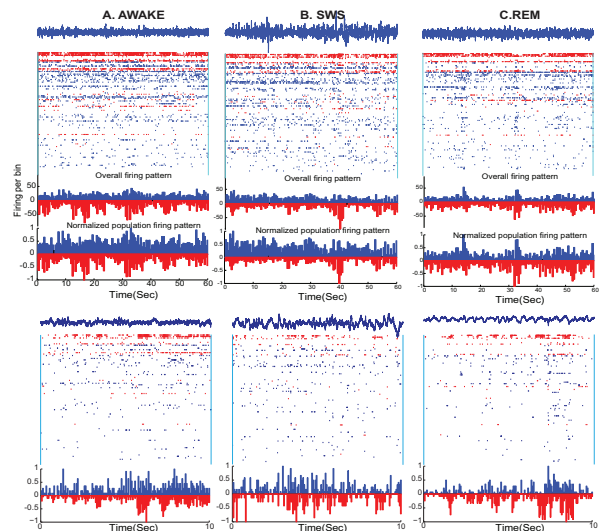


FIG. 2.— Sample recordings for awake (A), SWS (B) and REM (C) in human. Top row shows 60 seconds windows; bottom row shows a 10 second window of the same state. Putative inhibitory neurons (FS cells) are shown in red. Putative excitatory neurons (RS) are depicted in blue. In each panel, a sample LFP accompanies the spiking activity. Neurons are sorted based on their firing rate, within the portrayed epoch, in a descending order. Histograms show the overall excitatory activity. In the normalized histogram, overall activity is normalized to the maximum of firing rate (within FS or RS category) in the shown example. Zero lag correlation values are respectively: 0.726, 0.47 and 0.503.

bition follow each other's fluctuations.<sup>1</sup> This evidence shows that information processing rides on top of a multiscale balance. When the scale changes, the behavior of the fluctuations stays similar, which is another evidence for scale invariance in this system.

We also evaluated the behavior of the correlations between excitation and inhibition across different temporal scales. As shown in Fig.4, the ensemble FS and RS series showed well correlated dynamics. This type of ensemble correlation was observed across the multiple timescales. Further, the Monte Carlo randomization (four different types of randomization were implemented) showed that such correlation can not be due to aggregation of spike series into ensembles (For details of ensemble cross-correlogram and the randomization tests, see methods). The observed ensemble temporal interdependence, was seen in different subjects with different number of FS and RS cells yet with the similar relative RS/FS ratio of 4 to 1 (Fig.4A1-A4), was multiscale (Fig.4B1-B4), and was observed in all states (Fig.4C1-C4). The percentage of co-occurrence of spikes (in the ensemble series) at the lag zero and the maximum observed percentage of co-occurrence (whether that maximum was at lag 0 or not) showed a robust multiscale linear relationship. A first degree polynomial fit to the pooled values of lag zero vs maximum observed correlation, yielded a cross-subject average of  $0.9988 \pm 0.0134$  for Awake,  $0.9985 \pm 0.0147$  for

<sup>1</sup> When the ensemble activity is expressed in Hertz, the E and I ensemble activities are scaled mirrored images of each other. One reason could be that we are subsampling the possible space of neurons and therefore we can only find estimates of balance in experimental data. The true scaling of balance could only be calculated if and only if activity of all excitatory and inhibitory neurons are measured; a challenge that is not met with current technology but perhaps achievable in near future.

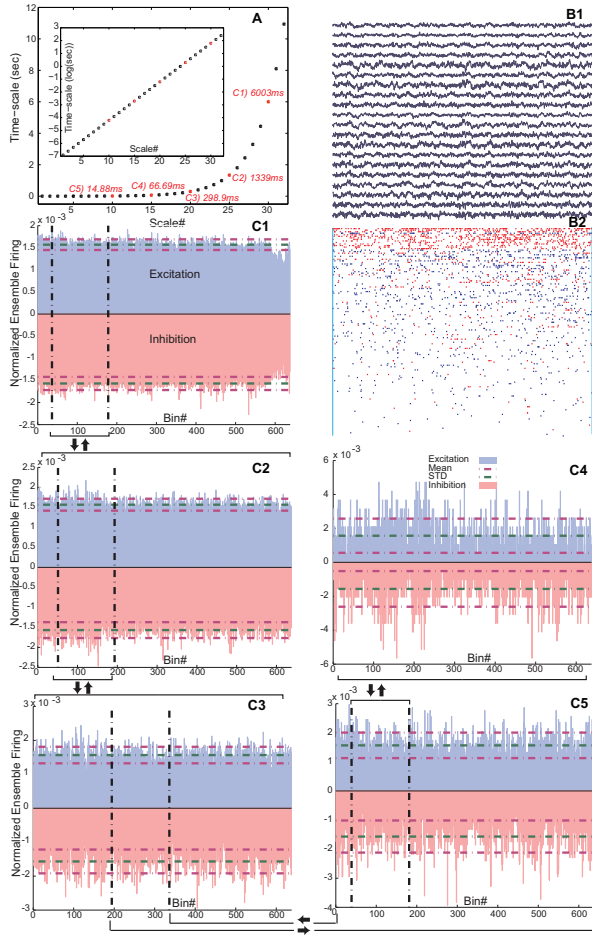


FIG. 3.— Preservation of excitatory-inhibitory balance across scales shows mirrored activity for different lengths of times (scales), in awake monkey. Note that the minus sign is only used conventionally to represent the opposing nature of excitation and inhibition. A. Definition of multiple scales used in the calculations. The scales were equally spaced in a logarithmic fashion. Those highlighted in red are shown in the example from monkey data in panels C1 through C5. Panels B1 and B2 show a sample 10 second of awake recordings’ local field potential and ensemble spiking, respectively. In B2, as before, red units are FS (Fast-spiking, putative inhibitory) and blue units are RS (Regular-spiking, putative excitatory). Panels C1 to C5 show ensemble activity of excitation (blue) versus inhibition (red) at multiple scales. In each panel, the ensemble firing of a given cell category is normalized by the total firing power in the same category during the shown epoch. For example, in panel C1 representing scale 30, each bin is about 6003 (sec) and total of 656 bins, show a duration of 1.0938 hr. Then a window of this epoch was chosen and zoomed in (scale 25) as shown in panel C2. The chosen window has exactly the same number of bins in scale 25. The ensemble firing of FS and RS in the 25th scale epoch was then normalized by the total firing of the FS and RS within this 656 bin epoch. Panel C3 to C5 are the next steps of zooming in (note the arrows showing the consecutive steps) the scales 20, 15 and 10. Again, in each step, exactly 656 bins of that scale are shown (and used for normalization). The mean and standard deviations are shown with dashed green and magenta lines, respectively. The ensemble activity shows a remarkable multiscale balance.

REM,  $0.9985 \pm 0.0162$  for light-sleep and  $0.9977 \pm 0.02539$  for slow-wave sleep. This tight linear relationship shows that the maximum of cross-correlograms was always very close to the zero lag, for all scales.

Multiscale distribution of magnitude and frequency of E-I ensemble fraction activity shows a general bal-

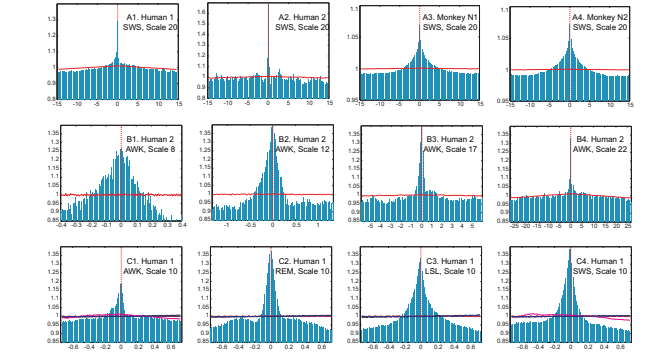


FIG. 4.— Excitation and inhibition are correlated over multiple scales. In each panel, the cross-correlogram is shown as the histogram of delays of the spikes in the ensemble target series (inhibitory) with respect to the spikes of the reference series (excitatory). The vertical dashed line shows the lag zero, the horizontal line shows the average ensemble cross-correlogram of the Monte Carlo randomized process. In each histogram, the count of delays is turned into percentage (y-axis) for comparative reliability across different subjects (with different number of cells), different scales (different bin sizes) and different states (different length of the event). Note that in all panels lags  $-50$  to  $+50$  are shown. However, the span of time (x-axis, in sec) depends on the bin size of the evaluated timescale. A1 to A4, Ensemble cross-correlograms during slow-wave sleep across two different humans and two different nights of recording from the monkey are shown for a sample timescale. The shown randomized control (red) is the average of 100 realization of random permutation of the ensembles (see methods). B1 to B4, Ensemble cross-correlogram during wakefulness for a given subject across four different scales. Note that in each histogram of delays, the same number of lags ( $-50$  to  $+50$ ) are tested. For a given scale, the size of the bin relates to the temporal expanse of that scale (as defined in Fig.3). The randomized control (red) is the average of 100 rounds of realization of random local jitter (see methods for details). C1 to c4, Ensemble cross-correlogram of different states in another human subject for an example scale. The randomized controls show that all four different randomization procedures yield highly reliable dispersion of events in the ensemble series such that the ensemble cross-correlogram no longer shows any temporal interdependency between the ensemble excitatory and inhibitory series.

ance between the two interacting systems. This evidence for multiscale balance is depicted in Fig.5A. Whether in SWS or wakefulness, the two systems show an astounding symmetrical distribution of magnitude and frequency of the ensemble fraction of excitation and inhibition. The estimated cross-subject average skewness,  $\gamma = E \left[ \left( \frac{X-\mu}{\sigma} \right)^3 \right]$ , for different states were close to zero (in the case of absolute symmetry):  $-0.013 \pm 0.046$  (awake),  $-0.012 \pm 0.087$  (slow-wave sleep),  $-0.010 \pm 0.015$  (light sleep) and  $0.052 \pm 0.015$  (REM). This Eiffel tower like symmetry shows that the balance is preserved across the scales. Naturally, as one approaches the coarse temporal scales, the distribution shrinks while still preserving the E/I balance (inset).

If balance were to be dynamic, the neocortical computation should portray the capability of keeping the excitation and inhibition in check (as shown above) (Renart *et al.* 2010) while hosting moment to moment transition in favor of one force or the other. As a result, the system should show moments of excitation dominance that are cancelled by moments of inhibition dominance and this feature should extend across all scales. The distribution of ensemble difference Fig.5B exactly exhibits this feature in a state-independent manner. Naturally, as one approaches the larger scales,

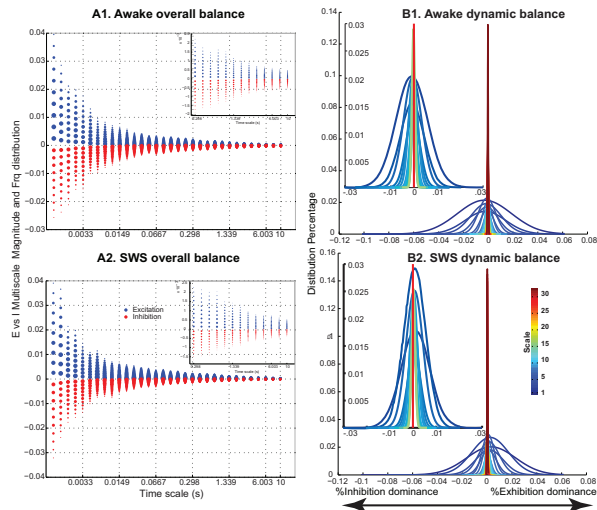


Fig. 5.— A1,2. Multiscale histogram of ensemble excitation (blue) versus inhibition (red) for the AWAKE and slow-wave sleep (SWS) in human A (Human REM and LSL (light sleep) as well as Monkey SWS and AWAKE had similar features, not shown here.). In each panel, there are 32 columns, each representing a given scale (as defined in Fig. 3.a). Each column represents the histogram of excitation (blue on top) and inhibition (red in bottom). The position of the circles refer to different magnitudes (increasing outward), and the diameter of each circle shows the frequency at which that given magnitude occurred. The insets are just for the visualization of the higher scales, to avoid overplotting of red and blue circles. In all cases, a clear symmetry is observed across multiple scales. Mean absolute value deviation,  $\frac{1}{n} \sum_{i=1}^n |x_i - \bar{X}|$ , a statistical measure of dispersion for different states were 0.0023 $\pm$ 0.0030 (awake), 0.0027 $\pm$ 0.0034 (slow-wave sleep). Light sleep and REM, not shown here, had similar structure and statistical dispersion, 0.0021 $\pm$ 0.0024 and 0.0028 $\pm$ 0.0032 respectively. B1,2. Multiscale distribution of Excitatory versus Inhibitory dominance. In all different states, as the timescale increases, the magnitude of the ensemble fraction activity for both E and I become closer and closer to each other. The result is that while one system may still dominate, the deviation from absolute balance gets smaller and smaller. At the very high time-scales, while the distribution narrows, the shape of the distribution stays true to its features in the fine temporal scales. Note that the time-scales are color-coded (The insets shows a zoom into higher scales).

the extent to which the dynamic interplay fluctuates narrows.

Although balance of E/I seem to be a hallmark of cortical computation, there is a large parameter space within which the input can be computationally processed while the balance is preserved (Xing & Gerstein 1996). While the distributions of ensemble fraction difference are more or less symmetric gaussian shaped, we have to emphasize that they do not follow normality in all cases. An example is shown in supplementary Fig. 9. If the data had come from a normal distribution, the values should follow the linear trend (shown in red). It is noticeable that in some cases, the tail ends deviate from normality and that the degree of this deviation is different from scale to scale. This deviation, which is further quantified in the text, could be due to reasons such as suboptimal sampling of units or more importantly the effects of slow oscillations on the spiking organization. Overall, the analysis shows that, although small deviations appear in deep SWS, the general balance was respected at all scales, and for all wake and sleep states. This aspect is further investigated in the next section.

### 2.3.2. State-dependent properties of balance

Though the system shows the core features of static and dynamic balance, our observations hint that departure from pure balance is an inherent feature of the system. We further quantified such departure based on the symmetry of the observations and that of the joint probability space. The complementary methods are shown in supplementary Fig. 10. Panel a, shows the implementation of weighted robust regression in order to calculate the angle between the symmetry axis of E-I ensemble activity vs the space axis of absolute symmetry. In parallel, we created a space in which for any given scale, the fraction of excitation, the fraction of inhibition, and their joint probability for all times  $t$  are morphed into a surface (supplementary Fig. 10b,c,d). Here, the deviation of the mid-plane of E/I ensemble activity from the plane of absolute symmetry is used to determine the degree of departure from absolute balance (see methods for details). As mentioned above, deviations of E-I ensemble fraction activity from absolute symmetry are a core feature of dynamic aspects of multiscale balance. A nonparametric two-sample Kolmogorov-Smirnov test,  $D_{n,n'} = \max_x |F_{AWAKE,n}(x) - F_{SWS,n'}(x)|$  where  $F_{AWAKE,n}$  and  $F_{SWS,n'}$  are the empirical cdfs of the normalized E/I ratio distributions for the two states, rejected ( $P_{val} \ll 10^{-3}$ ) that they come from the same distribution at the significance level of  $\alpha = 0.01$ . This shows that the degree of balance deviation is state-dependent. As portrayed in the Fig. 6, the highest degree of deviation from perfect balance happens during SWS. This higher degree of deviation from balance during sleep could be attributed to the fluctuations of inhibitory/excitatory activity during up-state and down-state (Renart *et al.* 2010; Steriade *et al.* 1993; Shu *et al.* 2003; Xue *et al.* 2014), as hallmarks of a bistable regime where toggling between the two states is enforced by the mutual excitation and feedback inhibition (Wilson & Cowan 1972). Transient stability of both up and down states is the other side of the coin characterized by a rhythmic transition between quiescent and active states (Holcman & Tsodyks 2006). This property, leads to the observed higher degree of deviations from absolute balance plane.

### 2.4. E/I imbalance during seizures

It has been speculated that the breakdown of excitation and inhibition could lead to epilepsy. The idea that the lack of inhibition or excess of excitation can cause seizure is not a new one (Symonds 1959). This has been experimentally used to induce or control seizure. For example, using optogenetics, epileptiform activity could be controlled by inducing inhibition (Krook-Magnuson *et al.* 2013; Paz *et al.* 2013; Tønnesen *et al.* 2009). Some other optogenetic studies even relate cortical E/I imbalance to other diseases such as mood disorders (Yizhar *et al.* 2011). However, it has been argued that such a clear-cut idea of lack of inhibition or excess inhibition as the major frame of epileptogenesis is perhaps misleading (Engel 1996). Here, we provide an example of a seizure recorded in one of our patients and show how E/I balance changes in a complex fashion that is in contrast to the simple misbalance scenario described above (see Fig. 7A,B). While an overall misbalance happens, throughout the seizure, some excitatory cells and some

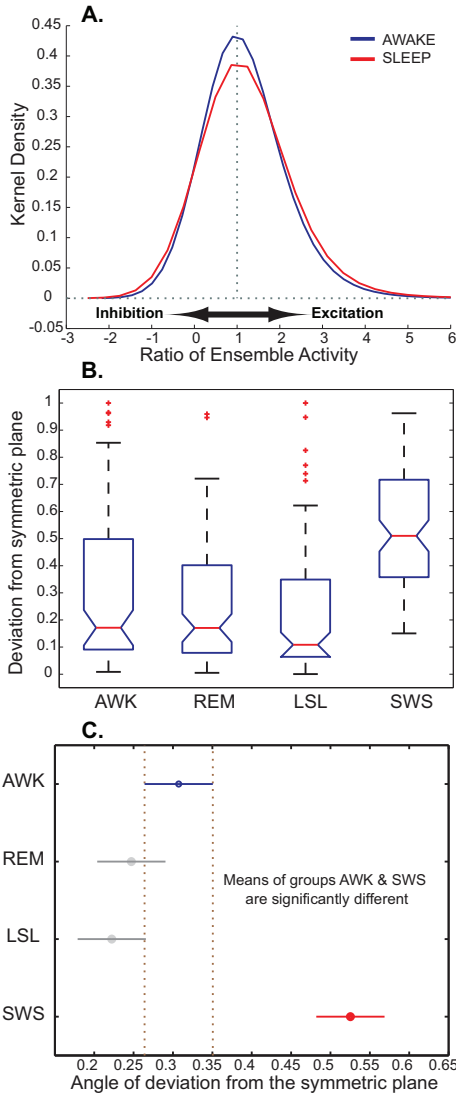


FIG. 6.— Panel A, kernel density of the ratio of E/I for the monkey awake and sleep states. Perfect balance (where the magnitude of ensemble matches) would be represented by the vertical dotted line ( $= 1$ ). Though the qualitative symmetry in each state is preserved, the kernel density estimates of sleep and awake do not match, with more kurtosis in awake and broader shoulders in sleep. A Two-sample Kolmogorov-Smirnov test on the E/I ratio at the significance level of  $\alpha = 0.01$ , rejected ( $P_{val} \ll 10^{-4}$ ) the null hypothesis that the data in awake and sleep are from the same continuous distribution. This is matched with the observations in humans, where the angle of deviation from the symmetric plane/axis is more pronounced during sleep rather than in awake (panel B). In the boxplot, the notch represents the median, the box boundaries show the lower and upper quartile and the asterisk show the outliers. In a multiple comparison test, panel C, awake and sws show statistically significant differences between their means ( $P_{val} \ll 10^{-3}$ ). Note that only slow-wave sleep shows significant statistical difference with the other states at  $\alpha = 0.05$ .

inhibitory cells increase their firing while some decrease or even stop firing. Particularly during the initial parts, the inhibitory cells dominate which is further followed by re-emergence of balance toward the end. Heatmaps of normalized ensemble excitatory and inhibitory, Fig.7C, show that the interplay between the two populations harbors a multiscale feature during the misbalance. The same multiscale breakdown of the balanced excitatory-inhibitory activity was observed for all seizures from two

human patients. Further studies are needed to decode the features of this complexity across many seizures and seizure types. See Ahmed et al. (personal communication) for a thorough quantification of the RS and FS cells during seizures, including the evidence for depolarization block.

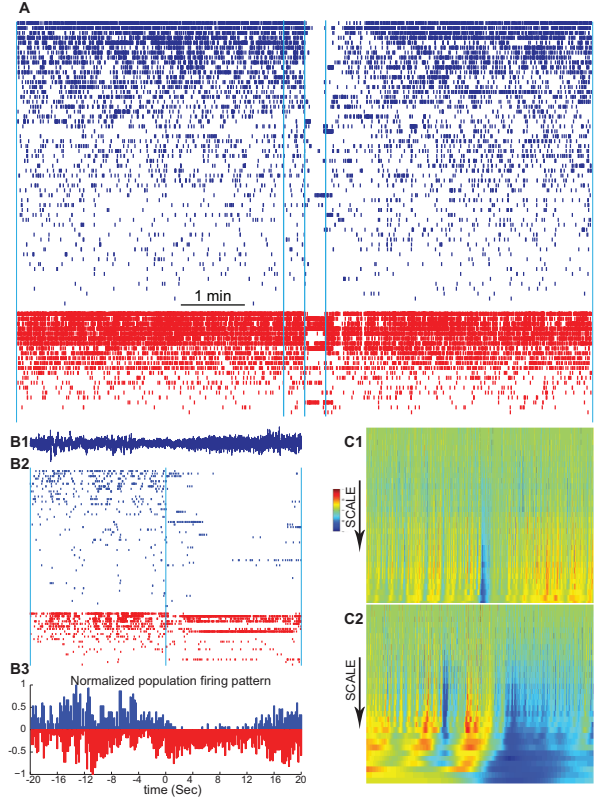


FIG. 7.— Misbalance in an example seizure recording in human. Panel A shows a 9 minute recording. Panels in B are the zoomed in version (the middle 40 seconds) of the same epoch (shown with the vertical lines in A). RS cells are in blue and ranked based on their firing rate within this epoch. Red cells show FS cells and are ordered according to their class firing rate. B1, LFP activity in the zoomed period, corresponding to B2 raster of FS and RS cells. B3, Normalized mirrored histogram showing where the misbalance occurs. C1, Heatmap of the normalized ensemble excitatory and inhibitory differences, corresponding to the 9 minute recording shown in A. C2 is the zoomed in version of the middle 40 seconds (corresponding to panels in B). Seizure happens around the mid-point and is visually distinct from the rest of the recording. During the seizure, a clear misbalance occurs; however it shows complex multiscale characteristics.

### 3. DISCUSSION

In this paper, we took advantage of the recent advances in the separation of excitatory and inhibitory cells, which were confirmed by direct cell-to-cell interaction (Peyrache et al. 2012). Our present analysis demonstrates that the excitatory and inhibitory neural populations are balanced in two cortical areas of human and monkey. This balance extends to multiple scales, as shown by the distributions of ensemble magnitudes (see Fig.3 and Fig.5A). We also found that the balance extends to nearly all brain states, and breaks down only during epileptic seizures. This breakdown suggests that the balance of excitatory and inhibitory activities is im-

portant for normal brain function and sleep. It also provides an important indication that the discrimination of excitatory and inhibitory neurons was successful.

The multi-scale characteristics of E/I suggests that the system is more complex than a perfect balanced activity. In fact, it has been shown that the spike timing itself seems to be finely tuned by dynamic interactions between excitatory and inhibitory conductances (Higley & Contreras 2006; Rudolph *et al.* 2007). In other words, the state of the system at a given point defines its capacity for responding to incoming stimuli. At fine time scales, the system may momentarily show either inhibitory or excitatory dominance (as in Fig.5A). However, the overall balance is always preserved, and this is true for wakefulness, REM or NREM sleep. Such properties also show that the system is not dominated by particular periodicities but seems to be broad-band (Fig.6). Naturally, as we move toward coarser and coarser time scales, the system becomes more and more rigid to the point that the gaussian shaped curves collapse and approach zero, i.e. equal power. It would be interesting to further characterize this momentary imbalance in future work, and the possible behavioral correlates of such imbalance.

Balance of excitation and inhibition has gone through many different renditions (Okun & Lampl 2009), from simulations based on random walk models (Gerstein & Mandelbrot 1964), to opposing views of balanced synaptic input (Shadlen & Newsome 1994; Softky & Koch 1993) and later to those relating it to synchrony (Stevens & Zador 1998), and those providing intracellular evidence for dynamic interplay between inhibition and excitation (Rudolph *et al.* 2007; Monier *et al.* 2008). However, for the first time, we show evidence of E/I balance in terms of network activity, estimated from large ensemble of units. The law of requisite variety expresses that high number of states of control elements are required to keep the controlled system in lesser number of stable states Ashby (1958). In complex systems, both scale and variability are necessary to keep a system in stable modes of operation and at every scale, variability is a must to provide adaptability (Bar-Yam 2004). The dynamics we see here seem consistent with such complex systems.

### 3.1. Summary

We suggest that the nervous system resides at a unique position in its state space, where unit firing in cortex, during wakefulness and sleep, reflects an overall preserved excitation-inhibition balance, but with highly rich dynamics across multiple temporal scales. This balance can tip one way or the other, and depending on the state of the system, can deviate from balance with different degrees of intensity. While the balance perturbation happens more regularly at finer temporal scales, it also transcends to other temporal scales of the system in a state-dependent fashion. When this multiscale dynamic balance breaks down, complex disorders such as epilepsy emerge (Fig.7). This is the signature of a system with many computational length scales, lending itself to a form of multiscale invariance.

## 4. METHODS

### 4.1. Recordings

Recordings of the ensemble neural activity were obtained through the implants of multielectrode arrays (Neuroport/Utah electrodes, Blackrock Microsystems). These arrays are composed of 100 electrodes arranged in a 10x10 matrix with an inter-electrode distance of 400 microns. For more details on electrodes see (Campbell *et al.* 1991; Jones *et al.* 1992). The patients, who were implanted, suffered from intractable seizures and were under neurosurgical monitoring to localize the focus of their epileptic seizure. The electrodes tips reached layer III of the neocortex (For details of implants see, (Truccolo *et al.* 2011). In the monkey, the implant was in the dorsal premotor cortex (PMd). Recordings were made during the performance of a motor task as well as during sleep. For details of implantation see (Dehghani *et al.* 2012; Truccolo *et al.* 2010).

As has been described previously, the spikes of putative excitatory (Regular Spiking., RS) neurons tend to be broader than putative inhibitory (Fast Spiking., FS) neurons (McCormick *et al.* 1985; Barthó *et al.* 2004). The recordings, were then spike-sorted and the units were categorized as either RS or FS. This categorization was based on morpho-functional characteristics of the spike-waveform and putative mono-synaptic connections (for details of such techniques see (Barthó *et al.* 2004; Peyrache *et al.* 2012). A Variety of extracted features describing the shape of the average spike waveform were used, such as half-width of the positive peak, half-width of the negative peak, interval between negative and positive peaks (valley-to-peak) and the ratio of the negative to positive peak amplitude. Based on these parameters, we classified the spike waveforms of all neurons into two groups using a standard K-means clustering algorithm. The procedure was repeated for each recording session separately; the neurons that were not assigned consistently to the same group were removed from further analysis.

### 4.2. Multiscale temporal rescaling

We used 32 different time scales to remap the ensemble activity to renormalized time-series of excitation and inhibition. For this process, spikes of ensemble excitatory group were binned at different time-scales. As the number of excitatory and inhibitory neurons in each recording differs from one another (even though their relative size  $4/1$ , is close to the anatomical observations), these values were normalized by the number of the neurons in each category of cells to obtain the ensemble fraction. This condition would overcome the limitations arising from both sub-sampling (here, 100s of neurons out of many thousands) and spatial non-uniformity of sampling (although the recording electrode is a regular grid, unit recordings are not always regularly spaced). The same process was repeated for inhibitory neurons. The results yielded ensemble fractions of inhibition and excitation at many different time scales. These time scales were distributed with regular spacing in logarithmic scale, ranging from ms to 10s of seconds. The logarithmic scale was chosen to have denser distribution at finer temporal resolution and avoid the computational redundancy at the

very coarse-grained level.

#### 4.3. Ensemble cross correlation

We first created the ensemble pool of the FS and RS cells in each subject of the study. The two series were lined up temporally along a common time axis. The ensemble RS and FS cells were used as the reference and target series respectively. For a given temporal scale, the bin length was defined according to the size of that scale as in Fig.3A. For each spike in the reference ensemble series, the delays of the spikes in the target ensemble series within -50 to +50 bin lags were calculated. Next, the collective count of target spikes within a given lag was defined as the value of ensemble cross-correlogram between FS and RS series. This value was turned into a percentage for enabling the comparison across subjects with different number of neurons, multiple scales with a different number of aggregate of spikes, and different states with different duration of events. This process was realized for all scales.

##### 4.3.1. Randomization

Randomization was used to construct control for the ensemble cross-correlogram. We used four different systems of randomization to test for different within and between aspect of ensemble series. Any of the randomization protocols was realized 100 times. For each randomization category, the average of 100 random ensemble cross-correlogram was used as the control for verification of the observed patterns in the non-randomized cross-correlogram.

- *Random permutation of ISI in the ensemble series.* After pooling all the FS and RS cells into their ensemble series, the ensemble ISI (inter-spike interval) was calculated. Then, for each of the two ensemble series, a random permutation of its ISI was followed by cumulative summation of ISI, resulting in the new temporal order of ensemble spikes. This procedure guarantees that the randomized ensemble series has the exact number of spikes and exact set of ISIs as of the original ensemble series, albeit with different temporal arrangement of spikes within a given ensemble series.
- *Circular shift of spike ensemble.* In this type of randomization, the spikes were first pooled to create the ensemble FS and RS series. For each series, the ISI of the ensemble series was calculated. Then all the spikes in each series were shifted at once with a random value between the lower bound (1) and upper bound (maximum of the ISI in the ensemble series). In each randomization trial, it was made certain that the degree of the shift was not equal for the two FS and RS ensemble, guaranteeing that the temporal relation of the two series was never repeated. In contrast to the previous procedure (random permutation), this randomization kept the temporal of order of spikes within each ensemble series same as the non-randomized series. However, here the temporal relation of the two FS and RS ensembles was disrupted.
- *Fixed-ISI circular shift of spikes.* Before aggregating the spikes into the ensemble series, the ISI of

each unit's spike series was calculated. Then the spikes of the unit were shifted based on a random value drawn between the lower bound (1) and upper bound (maximum of the ISI of the that unit's spike series). Next, all the randomized units were aggregated to create the randomized ensemble series. This procedure guarantees that the resultant ensemble series is constructed from units with intact internal structure of their spike timing but with a disrupted between-unit timing.

- *Local jitter randomization of spikes.* Next we tested the effect of randomization based on the statistics of each individual neuron before their aggregation to the ensemble series. First, the ISI of each FS (or RS) unit was calculated. Then the pool of the ISI as well as the ensemble of FS and RS was created. Next, each spike in the ensemble was shifted according a random number which was generated as the standard deviation plus a randomized (between -1 and 1, not including 0) multiple of the mean of pooled ISI. If the drawn random value was negative, the spike was shifted to the left and if the random chosen value was positive, the shift was toward the right in the ensemble series. This randomization, guarantees a tightly regulated data-driven local randomization based on the statistical properties of individual spikes.

#### 4.4. Deviation from absolute symmetry

We used complementary methods to calculate the deviation from symmetry between excitatory and inhibitory activities. First, we estimated the data-derived axis of symmetry based on the weighted bisquare robust regression. Then the angle between this axis and the identity line was used to represent the degree of deviation from pure symmetry. In parallel, for each time-scale, and for a given state, the time series of ensemble spiking data were reshaped into a 3-dimensional surface where the dimensions were the fraction of excitation, the fraction of inhibition, and number of their occurrences. As the durations of different states (SWS, REM, Wakefulness) differ from each other, the joint probability of ensemble fractions were also normalized by the whole length of the state to provide comparable results for further quantifications; i.e., the result is a surface in the 3D space of the fraction of excitation, the fraction of inhibition, and their joint probabilities. These surfaces were then Z-scored and their major orientation axis was calculated. Then the mid-point of the iso-surfaces along the major orientation axis was defined. Using orthogonal regression, a plane was fit to these point along the major orientation axis. This plane, is the plane of approximate symmetry of the data and divides the surface into two halves. In case of absolute balance at a given scale, the plane of symmetry of data would coincide with the symmetry plane of the 3D space. Deviations from perfect balance was calculated using the dihedral angle between the symmetry plane of data and symmetry plane of the 3D space. The results of the dihedral rotation was similar to the angle between axis of symmetry and the weighted least square regression (using robust bi-square fit) of the data in the 2D rendering of excitation fraction and inhibition fraction.

## 5. ACKNOWLEDGEMENTS

Nima Dehghani is an institute fellow of the Wyss Institute for Biologically-Inspired Engineering at Harvard University; he was previously funded by the Ecole de Neurosciences de Paris (ENP). The research

was funded by Centre National de la Recherche Scientifique (CNRS, France), Agence Nationale de la Recherche (ANR, France), European Community Future and Emerging Technologies program (BrainScales FP7-269921; The Human Brain Project FP7-604102) and National Institutes of Health (NIH grants 5R01NS062092, R01EB009282 and R01NS045853).

## REFERENCES

- ASHBY, WILLIAM. 1958. Requisite Variety and its implications for the control of complex systems. *Cybernetica*, **1**(2), 83–99.
- BAR-YAM, YANEER. 2004. Multiscale variety in complex systems. *Complexity*, **9**(4), 37–45.
- BARTHÓ, PETER, HIRASE, HAJIME, MONCONDUIT, LENAÍĆ, ZUGARO, MICHAEL, HARRIS, KENNETH D., & BUZSÁKI, GYÓRGY. 2004. Characterization of neocortical principal cells and interneurons by network interactions and extracellular features. *Journal of neurophysiology*, **92**(1), 600–8.
- CAMPBELL, PATRICK K., JONES, KELLY E., HUBER, ROBERT J., HORCH, KENNETH W., & NORMANN, RICHARD A. 1991. A silicon-based, three-dimensional neural interface: manufacturing processes for an intracortical electrode array. *IEEE transactions on bio-medical engineering*, **38**(8), 758–68.
- DEHGHANI, NIMA, HATSOPoulos, NICHOLAS G, HAGA, ZACH D, PARKER, REBECCA A, GREGER, BRADLEY, HALGREN, ERIC, CASH, SYDNEY S., & DESTEXHE, ALAIN. 2012. Avalanche Analysis from Multielectrode Ensemble Recordings in Cat, Monkey, and Human Cerebral Cortex during Wakefulness and Sleep. *Frontiers in physiology*, **3**(jan), 302.
- ENGEL, JEROME. 1996. Excitation and inhibition in epilepsy. *The Canadian journal of neurological sciences. Le journal canadien des sciences neurologiques*, **23**(3), 167–74.
- GERSTEIN, GEORGE L., & MANDELBROT, BENOIT. 1964. Random walk models for the spike activity of a single neuron. *Biophysical journal*, **4**(jan), 41–68.
- HAIDER, BILAL, DUQUE, ALVARO, HASENSTAUB, ANDREA R., & MCCORMICK, DAVID A. 2006. Neocortical network activity in vivo is generated through a dynamic balance of excitation and inhibition. *The Journal of neuroscience*, **26**(17), 4535–45.
- HIGLEY, MICHAEL J., & CONTRERAS, DIEGO. 2006. Balanced excitation and inhibition determine spike timing during frequency adaptation. *Journal of Neuroscience*, **26**(2), 448–457.
- HOLCMAN, DAVID, & TSODYKS, MISHA. 2006. The emergence of Up and Down states in cortical networks. *PLoS computational biology*, **2**(3), e23.
- JONES, KELLY E., CAMPBELL, PATRICK K., & NORMANN, RICHARD A. 1992. A glass/silicon composite intracortical electrode array. *Annals of biomedical engineering*, **20**(4), 423–37.
- KROOK-MAGNUSON, ESTHER, ARMSTRONG, CAREN, OIJALA, MIKKO, & SOLTESZ, IVAN. 2013. On-demand optogenetic control of spontaneous seizures in temporal lobe epilepsy. *Nature communications*, **4**(jan), 1376.
- LOMBARDI, FABRIZIO, HERRMANN, HANS, PERRONE-CAPANO, CARLA, PLENZ, DIETMAR, & DE ARCANGELIS, LUCILLA. 2012. Balance between Excitation and Inhibition Controls the Temporal Organization of Neuronal Avalanches. *Physical Review Letters*, **228703**(June), 1–5.
- MCCORMICK, DAVID A., CONNORS, BARRY W., LIGHTHALL, JAMES W., & PRINCE, DAVID A. 1985. Comparative electrophysiology of pyramidal and sparsely spiny stellate neurons of the neocortex. *Journal of neurophysiology*, **54**(4), 782–806.
- MONIER, CYRIL, FOURNIER, JULIEN, & FRÉGNAC, YVES. 2008. In vitro and in vivo measures of evoked excitatory and inhibitory conductance dynamics in sensory cortices. *Journal of neuroscience methods*, **169**(2), 323–65.
- OKUN, MICHAEL, & LAMPL, ILAN. 2009. Balance of excitation and inhibition. *Scholarpedia*, **4**(8), 7467.
- OKUN, MICHAEL, NAIM, AMIR, & LAMPL, ILAN. 2010. The subthreshold relation between cortical local field potential and neuronal firing unveiled by intracellular recordings in awake rats. *The Journal of neuroscience*, **30**(12), 4440–8.
- PAZ, JEANNE T., DAVIDSON, THOMAS J., FRECHETTE, ERIC S., DELORD, BRUNO, PARADA, ISABEL, PENG, KATHY, DEISSEROTH, KARL, & HUGUENARD, JOHN R. 2013. Closed-loop optogenetic control of thalamus as a tool for interrupting seizures after cortical injury. *Nature neuroscience*, **16**(1), 64–70.
- PEYRACHE, ADRIEN, DEHGHANI, NIMA, ESKANDAR, EMAD N., MADSEN, JOSEPH R., ANDERSON, WILLIAM S., DONOGHUE, JACOB A., HOCHBERG, LEIGH R., HALGREN, ERIC, CASH, SYDNEY S., & DESTEXHE, ALAIN. 2012. Spatiotemporal dynamics of neocortical excitation and inhibition during human sleep. *Proceedings of the National Academy of Sciences of the United States of America*, **109**(5), 1731–6.
- RENART, ALFONSO, DE, LA ROCHA JAMIE, BARTHÓ, PETER, HOLLENDER, LIAD, PARGA, NESTOR, REYES, ALEX, & HARRIS, KENNETH D. 2010. The asynchronous state in cortical circuits. *Science*, **327**(Jan), 587–90.
- RUDOLPH, MICHELLE, POSPISCHIL, MARTIN, TIMOFEEV, IGOR, & DESTEXHE, ALAIN. 2007. Inhibition determines membrane potential dynamics and controls action potential generation in awake and sleeping cat cortex. *J Neurosci*, **27**(May), 5280–90.
- SHADLEN, MICHAEL N., & NEWSOME, WILLIAM T. 1994. Noise, neural codes and cortical organization. *Current Opinion in Neurobiology*, **4**(4), 569–579.
- SHEW, WOODROW L, YANG, HONGDIAN, YU, SHAN, ROY, RAJARSHI, & PLENZ, DIETMAR. 2011. Information capacity and transmission are maximized in balanced cortical networks with neuronal avalanches. *The Journal of neuroscience*, **31**(1), 55–63.
- SHU, YOUSHENG, HASENSTAUB, ANDREA, & MCCORMICK, DAVID A. 2003. Turning on and off recurrent balanced cortical activity. *Nature*, **423**(6937), 288–93.
- SOFTKY, WILLIAM R., & KOCH, CHRISTOF. 1993. The highly irregular firing of cortical cells is inconsistent with temporal integration of random EPSPs. *The Journal of neuroscience*, **13**(1), 334–50.
- STERIADE, MIRCEA, NUEZ, ANGEL, & AMZICA, FLORIN. 1993. Intracellular analysis of relations between the slow (<1 Hz) neocortical oscillation and other sleep rhythms of the electroencephalogram. *J Neurosci*, **13**, 3266–83.
- STEVENS, CHARLES F., & ZADOR, ANTHONY M. 1998. Input synchrony and the irregular firing of cortical neurons. *Nature neuroscience*, **1**(3), 210–7.
- SYMONDS, CHARLES. 1959. Excitation and inhibition in epilepsy. *Proceedings of the Royal Society of Medicine*, **52**(6), 395–402.
- TØNNESEN, JAN, SØRENSEN, ANDREAS T, DEISSEROTH, KARL, LUNDBERG, CECILIA, & KOKAIA, MERAB. 2009. Optogenetic control of epileptiform activity. *Proceedings of the National Academy of Sciences of the United States of America*, **106**(29), 12162–7.
- TRUCCOLO, WILSON, HOCHBERG, LEIGH R., & DONOGHUE, JOHN P. 2010. Collective dynamics in human and monkey sensorimotor cortex: predicting single neuron spikes. *Nature neuroscience*, **13**(1), 105–11.
- TRUCCOLO, WILSON, DONOGHUE, JACOB A., HOCHBERG, LEIGH R., ESKANDAR, EMAD N., MADSEN, JOSEPH R., ANDERSON, WILLIAM S., BROWN, EMERY N., HALGREN, ERIC, & CASH, SYDNEY S. 2011. Single-neuron dynamics in human focal epilepsy. *Nature neuroscience*, **14**(5), 635–41.
- VRESWIJK, CARL VAN., & SOMPOLINSKY, HAIM. 1996. Chaos in Neuronal Networks with Balanced Excitatory and Inhibitory Activity. *Science*, **274**(5293), 1724–1726.
- WILSON, HUGH R., & COWAN, JACK D. 1972. Excitatory and inhibitory interactions in localized populations of model neurons. *Biophysical journal*, **12**(1), 1–24.

WILSON, KENNETH G. 1979. Problems in Physics with Many Scales of Length. *Scientific American*, 158–179.

XING, JING, & GERSTEIN, GEORGE L. 1996. Networks with lateral connectivity. I. dynamic properties mediated by the balance of intrinsic excitation and inhibition. *Journal of Neurophysiology*, **75**(1), 184–199.

XUE, MINGSHAN, ATALLAH, BASSAM V., & SCANZIANI, MASSIMO. 2014. Equalizing excitation–inhibition ratios across visual cortical neurons. *Nature*, **511**(7511), 596–600.

YIZHAR, OFER, FENNO, LIEF E, PRIGGE, MATTHIAS, SCHNEIDER, FRANZISKA, DAVIDSON, THOMAS J, O’SHEA, DANIEL J, SOHAL, VIKAS S, GOSHEN, INBAL, FINKELSTEIN, JOEL, PAZ, JEANNE T, STEHFEST, KATJA, FUDIM, ROMAN, RAMAKRISHNAN, CHARU, HUGUENARD, JOHN R, HEGEMANN, PETER, & DEISSEROTH, KARL. 2011. Neocortical excitation/inhibition balance in information processing and social dysfunction. *Nature*, **477**(7363), 171–8.

6. SUPPLEMENTARY FIGURES

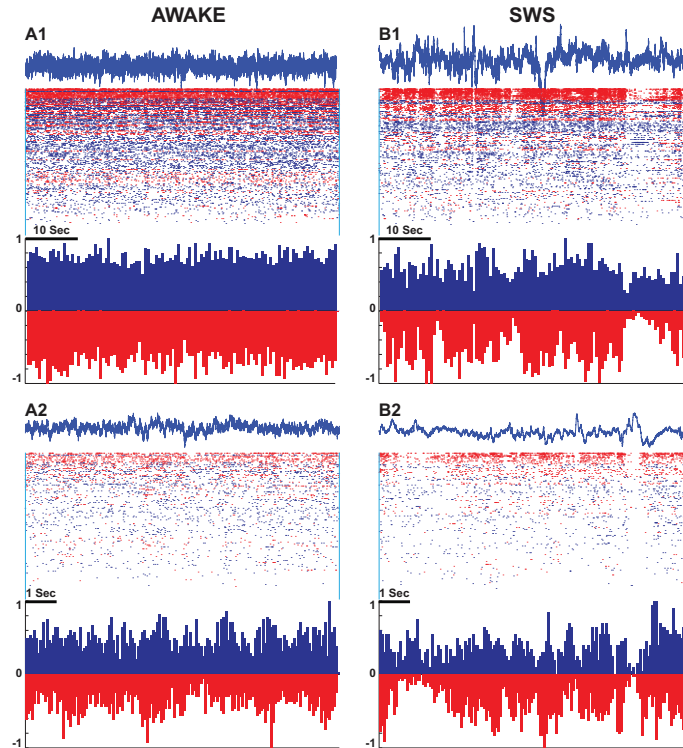


FIG. 8.— Sample recordings for AWAKE (left) and SWS (right) in monkey. A1 and B1 show 60 seconds windows; A2 and B2 show a 10 second window of the same state. In the rasters, putative inhibitory neurons (FS cells) and putative excitatory neurons (RS) are depicted in red and blue, respectively. In each panel, a sample LFP accompanies the spiking activity. Neurons are sorted based on their firing rate within the 60 sec epochs, in a descending order. Histograms show the overall excitatory activity normalized to the maximum of firing rate (within FS or RS category) in the shown example.

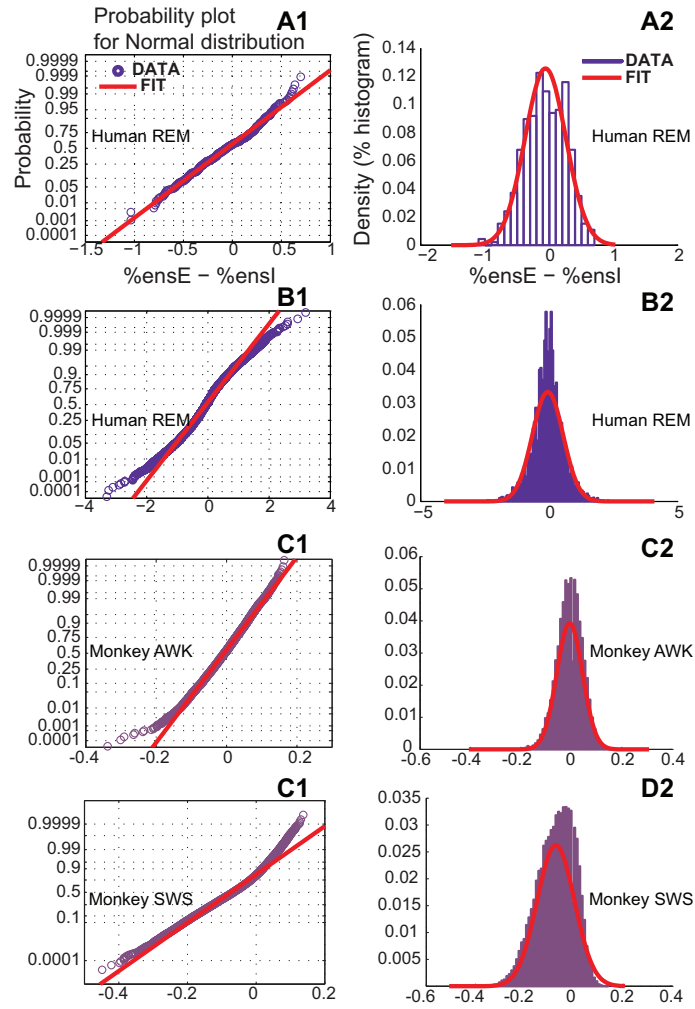


FIG. 9.— Panels in the left show normal probability plot of ensemble excitation and ensemble inhibition difference for, two sample scales from the same state (REM) in a human subject (A1 and B1) as well as two similar scales from different states (AWAKE and SLEEP) in monkey. Panels in the right show corresponding kernel density and histogram of ensemble difference. One can notice that although qualitative balance is noticeable, as in Fig.5, deviations from perfect normality is too an aspect of the system (tails of the distributions deviate from the straight line in red). As shown here, in some scales, deviation from perfect symmetry is different from scale to scale.

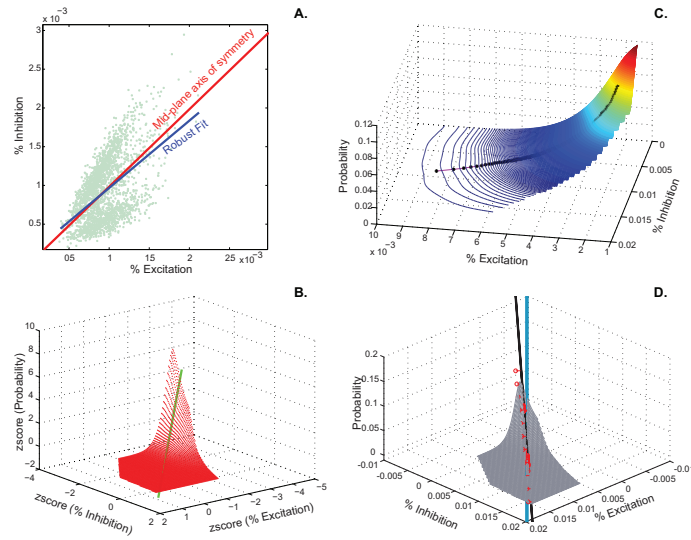


FIG. 10.— Panel A shows estimation of deviation from balance, between ensemble excitation and inhibition for a sample scale of SWS in a human subject, using robust bisquare regression. The fit (blue line) to the green cloud (data) show the axis of symmetry of the data. Its deviation from the symmetry axis of the plane (in red) shows the degree of balance deviation. Panels B to D show a different method for estimating the deviation from perfect symmetry. Panel B, shows the major orientation axis of the Zscored data. Panel C, shows the distribution of E-I ensemble fraction pairs for a sample scale during SWS. The black lines are the centroids of the iso-surfaces. Panel D, combining these info, one can find the mid-plane of the data (shown in black) and find its tetrahedral angle with the plane of absolute symmetry (shown in cyan). The distribution of such angles is shown in Fig. 6.